A&A 437, 537–543 (2005)
DOI: 10.1051/0004-6361:20041319

Astronomy & Astrophysics

Radio emission by particles due to pulsar spin⋆

R. M. C. Thomas and R. T. Gangadhara

Indian Institute of Astrophysics, Bangalore – 560034, India
e-mail: [mathew;ganga]@iiap.res.in

Received 19 May 2004 / Accepted 15 February 2005

Abstract. We present a relativistic model for the motion of charged particles in rotating magnetic field lines projected onto a plane perpendicular to the rotation axis. By making an approximation that the projected field lines are straight, an analytical expression is obtained for the particle trajectory. The motive behind developing this model is to elucidate some of the effects of rotation in pulsar profiles. There is significant contribution to the curvature of a particle trajectory due to the rotation of the pulsar, which is in addition to the inherent curvature of the field lines. The asymmetry in the observed pulse shapes can be explained by considering the aberration-retardation effects. The single sign circular polarization observed in many pulsars might be due to the relative orientation of sight line with respect to the particle trajectory plane.

Key words. pulsars general – radiation mechanisms: non-thermal – stars: rotation – magnetic fields – radio continuum: general

1. Introduction

The wide diversity in the radiation characteristics of pulsars makes it difficult to fully understand the emission process in the light of models that have been developed with some simplifying assumptions. Among all the many emission mechanisms, curvature emission has emerged as the most probable choice (Sturrock 1971; Ruderman & Sutherland 1975, hereafter RS75; Lyne & Manchester 1988; Gil & Snakowski 1990). In order to explain the high brightness temperature observed in pulsars, coherent emission by bunched particles has been postulated (Karpman et al. 1975; RS75; Buschauer & Benford 1977). Other models based on plasma effects have also been proposed for pulsar radiation (e.g., Melrose & Gedalin 1999; Asséo & Rozele 2000; Gil et al. 2004).

Most of these models emphasise explaining the high brightness temperature of pulsars, but leave the polarization poorly explained. However, polarization observations such as the polarization angle swing favors curvature radiation. It has been considered as a natural emission process for pulsars, though there are unresolved problems like bunch formation, orthogonal polarization modes, etc. (e.g., Stinebring et al. 1984; Gangadhara 1997; Gil et al. 2004).

It is imperative to understand the influence of rotation when closely studying the curvature emission mechanism. The idealized case of particle acceleration was discussed by Machabeli & Rogava (1994, hereafter MR94), who considered particles moving freely along an infinitely long, rigidly rotating straight tube and derived an expression for the trajectory of a particle. Gangadhara & Lesch (1997) proposed a model for the particle acceleration in rotating magnetosphere in the context of active galactic nuclei (AGN). Reiger & Mannhiem (2000) also discussed particle acceleration along the rotating straight magnetic field lines in AGN, by assuming that the angular velocity of particles is the same as that of AGN.

In the case of pulsars, Gold (1969) was the first to propose a pulsar emission mechanism based on rotation. This model was taken up further by many authors and found to encounter difficulties in explaining the interpulses (e.g., Sturrock 1971). Blaskiewicz et al. (1991) have studied the effects of corotation velocity on the pulsar radio emission by assuming a constant emission height. Hibschhman & Arons (2000) extended their work to include the first order effects to study delays in the phase of polarization angle sweep due to aberration. Later, Peyman & Gangadhara (2002) improvised the model of Blaskiewicz et al. (1991) by relaxing the assumption of constant emission height, and then analyzed the effect of rotation on the morphology of pulsar profiles and polarization.

Gangadhara (1996, hereafter G96) derived the equation of motion of a charged particle in pulsar magnetosphere, and considered the straight field lines, which are projected onto a two dimensional (2D) plane placed perpendicular to the rotation axis. The dominant forces, which act on a particle moving along rotating the field lines, are the magnetic Lorentz force, centrifugal force, and coriolis force. The rotational energy of the pulsar is transferred to the corotating plasma as it moves along the field lines. The magnetic Lorentz force acts as a constraining force and drags the plasma along the field lines. Because of the inclination of the magnetic axis relative to rotation axis, corotating plasma tends to rotate with an angular velocity that is less than that of pulsar on some field lines.

⋆ Appendices A and B are only available in electronic form at http://www.edpsciences.org

The difference in the angular velocities of particle and pulsar had been already pointed out in RS75.

In the present work, a follow-up to G96, we consider the same 2D geometry and analyze the dynamics of a charged particle. Since the field line curvature radii of open field lines are comparable to the light cylinder radius, over a significant radial distance, we can approximate them to be straight lines.

In super strong magnetic fields, the drift velocity becomes negligible compared to the velocity parallel to the field lines. The Larmour radius of gyration becomes quite small, and hence particles almost stay on the same field lines all along their trajectories. This motion is considered as the bead-on-wire approximation. The particles are accelerated because of the unbalanced centrifugal force, and thus extract the rotational energy of the pulsar. The single particle emission is considered in this model, and we plan to consider the collective effects in later work. We take the non-uniform angular velocity of particles into consideration, which can be less than the pulsar angular velocity on field lines that are inclined with respect to the meridional plane. Since the particle trajectories are found to be curved, we estimate the curvature emission and analyze the effects of rotation on the radiation characteristics. In Sects. 2 and 3, we solve the equation of motion of a relativistic charged particle and find its trajectory. We compute the characteristic frequency of curvature radiation in Sect. 4. In Sect. 5 we estimate the polarization parameters and plot them with respect to different parameters.

2. Charged particle dynamics

We assume that the dipolar magnetic field lines are projected onto a plane perpendicular to the rotation axis. Consider an inertial Cartesian coordinate system as shown in Fig. 1, where the "z" axis is parallel to the rotation axis ($\hat{\Omega}$) of pulsar. The projected magnetic axis on the x–y plane coincides with the x-axis at time $t = 0$. The equation of motion for a charged particle moving along a rotating magnetic field line is given by (G96),

$$\frac{\mathrm{d}}{\mathrm{d}t}\left(m\frac{\mathrm{d}r}{\mathrm{d}t}\right) = m\Omega^{*2}r, \tag{1}$$

where $m = m_0\gamma$ is the relativistic mass, γ the Lorentz factor, m_0 the rest mass, Ω^* the angular velocity and r the radial position of a particle.

Let $V_r = \mathrm{d}r/\mathrm{d}t$ and $V_\phi = r\Omega^*$ be the components of particle velocity, then

$$\boldsymbol{\beta} = \frac{1}{c}(V_r\hat{e}_r + V_\phi\hat{e}_\phi), \tag{2}$$

where c is the speed of light. We define the unit vectors in the radial and azimuthal directions as

$$\hat{e}_r = (\cos\phi,\ \sin\phi,\ 0), \tag{3}$$
$$\hat{e}_\phi = (-\sin\phi,\ \cos\phi,\ 0), \tag{4}$$

where ϕ is the angle between the radial vector to particle and the x-axis. Then the Lorentz factor of particle is given by

$$\gamma = \frac{1}{\sqrt{1-\beta^2}} = \left[1 - \left(\frac{1}{c}\frac{\mathrm{d}r}{\mathrm{d}t}\right)^2 - \left(\frac{r\Omega^*}{c}\right)^2\right]^{-1/2}. \tag{5}$$

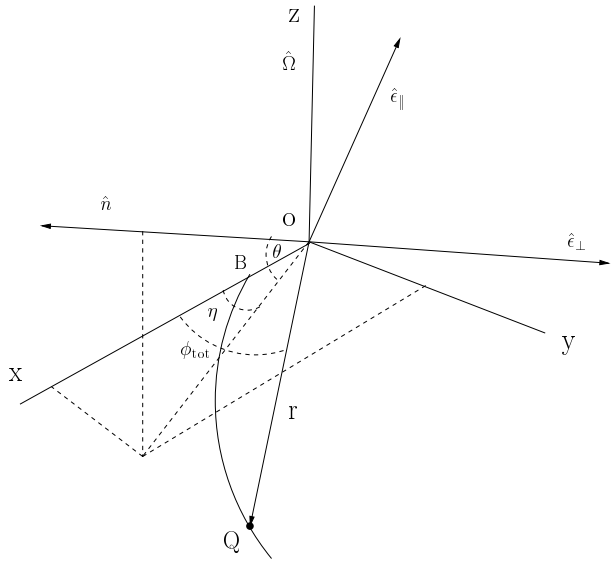

Fig. 1. The coordinate system in which the particle motion is considered. The curve BQ represents the particle trajectory in the x–y plane.

Then consider a particle injected at the point B onto a magnetic field line which is inclined by an angle ϕ_p with respect to the x-axis at time $t = 0$. Let $d_0 = \mathrm{OB}$ be the distance between B and the rotation axis. The effective angular velocity (G96) of a particle is given by

$$\Omega^* = \Omega\left[\frac{r^2 - d_0^2\cos^2\theta_0 - d_0\sin\theta_0\sqrt{r^2 - {d_0}^2\cos^2\theta_0}}{r\left(\sqrt{r^2 - {d_0}^2\cos^2\theta_0} - d_0\sin\theta_0\right)}\right]$$
$$= \Omega\sqrt{1 - \frac{b^2}{r^2}}, \tag{6}$$

where Ω is the angular velocity of pulsar, $b = d_0\cos\theta_0$ and $\theta_0 = (\pi/2) - \phi_\mathrm{p}$ is the angle between the field line tangent and $\hat{e}_\phi$ at B. Using the relation for Ω^*, we can write γ as

$$\gamma = \left[1 + D^2 - \left(\frac{1}{c}\frac{\mathrm{d}r}{\mathrm{d}t}\right)^2 - \left(\frac{r\Omega}{c}\right)^2\right]^{-1/2}, \tag{7}$$

where $D = \Omega d_0\cos\theta_0/c$. Thus, using the expression for γ, we rewrite Eq. (1):

$$\gamma\frac{\mathrm{d}^2r}{\mathrm{d}t^2} + \frac{\mathrm{d}\gamma}{\mathrm{d}t}\frac{\mathrm{d}r}{\mathrm{d}t} = \Omega^2\left(1 - \frac{b^2}{r^2}\right)\gamma\, r. \tag{8}$$

By multiplying Eq. (8) by $r/(\gamma c^2)$, and defining a dimensionless variable

$$s = \frac{\Omega}{c}\frac{r}{\sqrt{1+D^2}}, \tag{9}$$

we obtain

$$s\frac{\mathrm{d}^2s}{\mathrm{d}t^2} + \frac{\left[2s^2 - D^2/\left(1+D^2\right)\right]}{1-s^2}\left(\frac{\mathrm{d}s}{\mathrm{d}t}\right)^2 - s^2\Omega^2 + \Omega^2\frac{D^2}{1+D^2} = 0. \tag{10}$$

Since θ_0 is close to $\pi/2$ for the field lines, which are close to the x-axis, we find $D^2 \ll s^2$ for $d_0 < r$. Therefore, we reduce Eq. (10) by dropping the terms containing $D^2/1+D^2$, and obtain

$$\frac{\mathrm{d}^2 s}{\mathrm{d}t^2} + \frac{2s}{1-s^2}\left(\frac{\mathrm{d}s}{\mathrm{d}t}\right)^2 - s\,\Omega^2 = 0. \tag{11}$$

To find the solution of Eq. (11), we follow the method proposed by Zwillinger (1989). By choosing $f = (\mathrm{d}s/\mathrm{d}t)^2$, we can reduce it to the following form:

$$\frac{\mathrm{d}f}{\mathrm{d}s} + f\frac{4s}{1-s^2} = 2s\,\Omega^2. \tag{12}$$

Its solution is given by

$$f = \Omega^2\left(1-s^2\right) + C\left(1-s^2\right)^2, \tag{13}$$

where C is the integration constant. To find C we use the initial condition that at $t = 0$, it follows from Eq. (9) that $s_0 = s(0) = r_0\Omega/(c\sqrt{1+D^2})$ and $\dot{s}_0 = \mathrm{d}s/\mathrm{d}t|_{t=0} = v_0\Omega/(c\sqrt{1+D^2})$, where r_0 and v_0 are the particle's initial position and velocity. Therefore, we obtain $C = -\Omega^2 k^2$ and

$$k^2 = \frac{1}{1-s_0^2}\left[1 - \frac{\dot{s_0}^2}{(1-s_0^2)\Omega^2}\right]. \tag{14}$$

Hence Eq. (13) reduces to the following form

$$\frac{\mathrm{d}s}{\mathrm{d}t} = \Omega\sqrt{(1-s^2) - k^2(1-s^2)^2} \tag{15}$$

whose solution is given by

$$s = \mathrm{cn}(\lambda - \Omega\mathrm{t}), \tag{16}$$

where $\mathrm{cn}(z)$ is the Jacobian Elliptical cosine function (Abramowicz & Stegun 1972), and

$$z = \int_0^{\mathrm{sn}(z)} \frac{\mathrm{d}w}{\sqrt{(1-w^2)(1-k^2w^2)}}, \tag{17}$$

$$\lambda = \int_0^{\phi_0} \frac{\mathrm{d}\zeta}{\sqrt{1-k^2\sin^2\zeta}}, \tag{18}$$

$$\phi_0 = \arccos\left(\frac{r_0\Omega}{c}\right). \tag{19}$$

Using the expression for s given by Eq. (9), we find the radial position of the particle:

$$r = \frac{c\sqrt{1+D^2}}{\Omega}\mathrm{cn}(\lambda - \Omega\mathrm{t}). \tag{20}$$

The radial position of the particle according to Eq. (20) as a function of time is plotted in Fig. 2. It shows that the particle position increases with time and reaches a maximum at the distance of light cylinder radius $r_L = Pc/2\pi$, where P is the pulsar period. Next, the particle returns back to origin, due to the reversal of the centrifugal force. This type of oscillatory motion of a particle in an infinitely long, straight and rigidly rotating tube has been discussed by MR94.

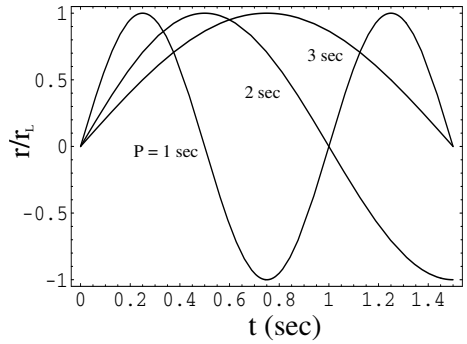

Fig. 2. Radial position of the particle as a function of time. Used $\gamma_0 = 100$, $d_0 = 10^6$ cm and $\theta_0 = 90°$.

Though we have extended the calculation of r of a single particle all the way up to light cylinder, it may not be realistic in the case of plasma motion. Near the light cylinder, plasma inertia causes the field lines to sweep back and break down of the rigid body motion. The Lorentz factor of a particle, which follows from Eqs. (7), (15), and (16), is given by

$$\gamma = \frac{1}{k\sqrt{(1+D^2)}\,\mathrm{sn}^2(\lambda - \Omega t)}. \tag{21}$$

3. Particle trajectory and its radius of curvature

In Fig. 3 we consider a particle moving along the field line BQ. The point A represents the particle injection point at time $t = 0$ that is at a distance d_0 from the rotation axis. The particle coordinates can be defined as

$$(x,\, y) = r(t)\,(\cos\phi_{\mathrm{tot}},\, \sin\phi_{\mathrm{tot}}), \tag{22}$$

where ϕ_{tot} is the angle between the radial vector to the particle and the x-axis. Based on Fig. 3, we define

$$\phi_{\mathrm{tot}}(t) = \Omega t \pm \phi'(t), \tag{23}$$

where

$$\phi'(t) = \cos^{-1}\left(\cos\phi_{\mathrm{p}}\sqrt{1 - \frac{{d_0}^2}{r^2}\sin^2\phi_{\mathrm{p}}} + \frac{d_0}{r}\sin^2\phi_{\mathrm{p}}\right). \tag{24}$$

For $d_0 \ll r$, we find

$$|\phi'(t)| \simeq |\phi_{\mathrm{p}}|. \tag{25}$$

The $\pm$ signs in Eq. (23) correspond to the sign of the angle ϕ_{p}. In Fig. 4 we have plotted the trajectories of the particles moving along different magnetic field lines, which are marked with ϕ_{p}. It shows that the trajectories are curved toward the direction of pulsar rotation. The particles moving in those trajectories are accelerated, and thus emit curvature radiation. The curvature radii of those trajectories slightly differ from one another, as the particle angular Ω^* is different for each field line.

To derive the curvature radii of the particle trajectory, we approximate $\mathrm{cn}(\lambda - \Omega\mathrm{t})$ and $r(t)$ using the formalism given by Pearson (1974):

$$cn(z,k) = \cos z + \frac{k^2}{4}(z - \sin z\cos z)\sin z + O(k^4). \tag{26}$$

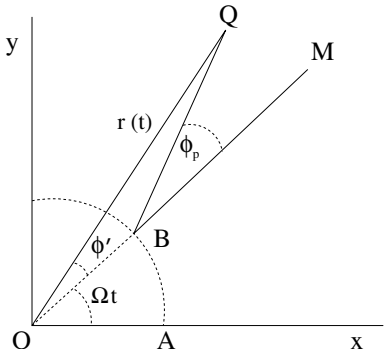

Fig. 3. The geometry of motion of a particle along a rotating field line BQ. The angles are ∠XOM = Ωt, ∠MBQ = ϕ_p and ∠MOQ = ϕ', and the radius OA = OB = d_0.

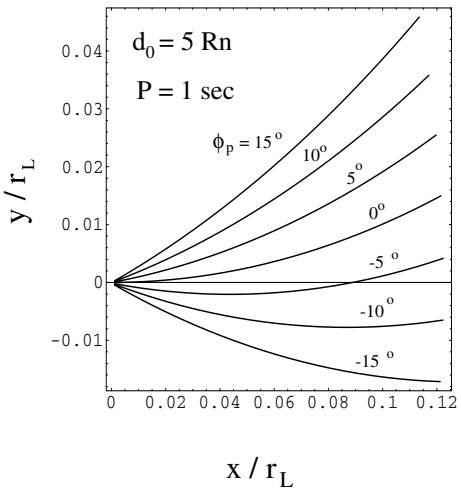

Fig. 4. Particle trajectories during the time interval $0 \le t \le 0.02$ s in laboratory frame. We considered the field lines which lie in the range of $-15^\circ \le \phi_p \le 15^\circ$ with an interval of 5°. Assumed neutron star radius $R_n \approx 10$ Km.

In the limit of $t \ll 1$ and $k \ll 1$, the series expansion of $r(t)$ is given by

$$r(t) = a_0 + a_1 t + a_2 t^2 + a_3 t^3 + a_4 t^4 ... \tag{27}$$

where a_0, a_1, a_2, a_3, a_4... are the expansion coefficients (see Thomas & Gangadhara 2005).

For $v_0 \approx c$, Eq. (14) implies $k \approx 0$. Therefore, using Eqs. (16)–(19), we find $\lambda = \pi/2$ and sn z = sin z. Thus, we have

$$r(t) \approx \frac{c\sqrt{1+D^2}}{\Omega} \sin(\Omega t). \tag{28}$$

Using the expression for $r(t)$ in Eqs. (22) and (25), we find the curvature radius of particle trajectory:

$$\rho = \frac{\left[(dx/dt)^2 + (dy/dt)^2\right]^{3/2}}{(dx/dt)(d^2y/dt^2) - (dy/dt)(d^2x/dt^2)} \approx \frac{1}{2} r_L \sqrt{1+D^2}. \tag{29}$$

It shows that the curvature radius of a particle trajectory is approximately $r_L/2$ for $\theta_0 = \pi/2$. However, for other values of θ_0, we find ρ becomes slightly larger than $r_L/2$. Note that these values of ρ are comparable to the intrinsic curvature radii of dipolar field lines in the emission region given by Gangadhara (2004). We find in the conal emission regions that the intrinsic curvature radii of field lines are comparable to the curvature radius induced by rotation on the particle trajectory. If the core emission is believed to come from the field lines that are close to the magnetic axis, then it becomes difficult to explain the core emission due to the intrinsic curvature of field lines. This is because the field lines that are very close to the magnetic axis have very large curvature radii, and for the magnetic axis it is infinity. Therefore, in the absence of rotation, we cannot expect any significant curvature emission from the particles or plasma moving along the field lines that are close to the magnetic axis. However, from the observations we do see many pulsars emitting strong cores. In our model we show that if we consider pulsar rotation the core emission can be explained, because the rotation induces significant curvature into the trajectory of particles which move along the field lines that are close to the magnetic axis.

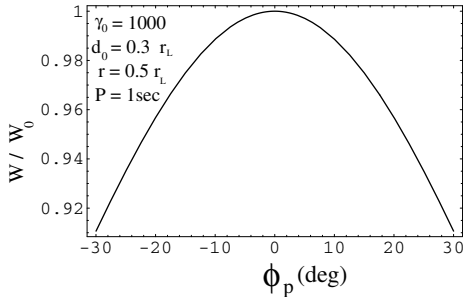

Fig. 5. The power emitted by a particle as a function of ϕ_p. The parameter $W_0 = 25.6 q^2\Omega^2/(3ck_0^4)$, and $k_0 = k$ at $D = 0$.

4. Radiation emitted by a particle

When the particles move along curved trajectories, they emit curvature radiation. The characteristic frequency of the curvature radiation is given by (RS75)

$$\omega_c = \frac{3}{2}\gamma^3 \left(\frac{c}{\rho}\right) \approx 3\,\Omega \frac{1+D^2}{k^3\left[1+D^2-(r/r_L)^2\right]^3}. \tag{30}$$

By knowing the γ and ρ from Eqs. (7) and (29), we can estimate ω_c. The total power emitted by a particle is given by

$$W = \frac{2}{3}\frac{q^2}{c}\,\gamma^4 \left(\frac{c}{\rho}\right)^2 \approx \frac{8\,q^2}{3\,c}\,\frac{\Omega^2(1+D^2)}{k^4[1+D^2-(r/r_L)^2]^4}, \tag{31}$$

where q is the particle charge. In Fig. 5, we plotted W as a function of ϕ_p at $r = 0.5\,r_L$. We find maximum power is emitted by the particles that move along the field line with $\phi_p = 0$ as $D = 0$, compared to those on the other field lines ($\phi_p \neq 0$).

5. Polarization of radiation

The radiation electric field is given by (e.g., Jackson 1972; Gangadhara 1997)

$$\boldsymbol{E}(\omega) = C_f \int_{-\infty}^{+\infty} \hat{n} \times (\hat{n} \times \boldsymbol{\beta}) \exp\{\, i\,\omega(t - \hat{n}\cdot\boldsymbol{r}/c)\}\, \mathrm{d}t, \tag{32}$$

where $C_f = -\mathrm{i}\omega\, q\, \mathrm{e}^{\mathrm{i}\omega S_0/c}/\sqrt{2\pi} S_0 c$, S_0 is the distance from the origin to observer, ω the radiation frequency and $\hat{n}$ the sight line. To solve the integral, we shall express $\hat{n} \times (\hat{n} \times \boldsymbol{\beta})$ (see Appendix A) and the argument of exponential as series expansions in time t. Consider the sight line which makes an angle θ with the 2D plane, and η with the x-axis:

$$\hat{n} = (\cos\theta\cos\eta,\ \cos\theta\sin\eta,\ \sin\theta). \tag{33}$$

To describe the polarization state of the emitted radiation, we define orthogonal unit vectors (see Fig. 1):

$$\hat{\epsilon}_\parallel = (-\sin\theta\cos\eta,\ -\sin\theta\sin\eta,\ \cos\theta), \tag{34}$$

$$\hat{\epsilon}_\perp = (-\sin\eta,\ \cos\eta,\ 0). \tag{35}$$

The unit vectors $(\hat{n},\ \hat{\epsilon}_\parallel,\ \hat{\epsilon}_\perp)$ form an orthogonal triad:

$$\hat{n} \times \hat{\epsilon}_\perp = \hat{\epsilon}_\parallel. \tag{36}$$

Let t_0 be the time at which $\boldsymbol{\beta}$ aligns with $\hat{n}$, and the observer receives radiation. We transform the time variable t to $t + t_0$ such that Ωt_0 stands for an initial phase. Thus, we find

$$r(t + t_0) = a'_0 + a'_1 t + a'_2 t^2 + a'_3 t^3 + a'_4 t^4 \ldots \tag{37}$$

based on Eqs. (26) and (27). The expansion coefficients $a'_0,\ a'_1,\ a'_2,\ a'_3,\ a'_4$ ... are same as $a_0,\ a_1,\ a_2,$ ... except λ replaced by $\lambda - \Omega t_0$.

Using Eqs. (20) and (22), we find the series expansion of the exponential argument in Eq. (32) and keep the terms up to the order of t^3:

$$\omega\left[(t + t_0) - \frac{\hat{n}.\boldsymbol{r}}{c}\right] = \omega\left[t + t_0 - \frac{r}{c}\cos\theta\,(\cos\eta\,\cos\phi_{\rm tot} + \sin\eta\,\sin\phi_{\rm tot})\right], = N_0 + N_1 t + N_2 t^2 + N_3 t^3 \ldots \tag{38}$$

where $N_0,\ N_1,\ N_2$ ... are series expansion coefficients (see Appendix C in Thomas & Gangadhara 2005). The series expansion of exponential argument is converging, and it is quite obvious from Eqs. (20) and (26). In the limit of $k \approx 0$, the series expansion of r behaves like the trigonometric sine function. Since the angular width of emission beam is $\approx 2/\gamma$, the time taken by the particle to cross the angular width of the order of emission beam is $\approx 2\rho/c\gamma$. Thus the truncation of higher order terms introduces a negligible error in our calculations. Since we intend to reduce the integral in Eq. (32) to a known form, we limit the series expansion terms up to the order of t^3.

Using the transformation given by Buschauer & Benford (1976), we find the electric field components (see Appendix B):

$$E_\parallel = \frac{1}{c}\,(V_{\parallel 0}B_0 + V_{\parallel 1}B_1 + V_{\parallel 2}B_2)\ C_f\, \mathrm{e}^{\mathrm{i}N_0}\ \sin\theta, \tag{39}$$

$$E_\perp = \frac{1}{c}\,(V_{\perp 0}B_0 + V_{\perp 1}B_1 + V_{\perp 2}B_2)\ C_f\, \mathrm{e}^{\mathrm{i}N_0}. \tag{40}$$

Next, we define the Stokes parameters as

$$\begin{aligned} I &= E_\parallel E^*_\parallel + E_\perp E^*_\perp, \\ Q &= E_\parallel E^*_\parallel - E_\perp E^*_\perp, \\ U &= 2\Re\left(E^*_\parallel E_\perp\right), \\ V &= 2\Im\left(E^*_\parallel E_\perp\right). \end{aligned} \tag{41}$$

The linear polarization is given by

$$L = \sqrt{Q^2 + U^2}. \tag{42}$$

In observations, pulsar polarization is normally expressed in terms of L and V. So, in our model, we call L and V polarization parameters.

5.1. Polarization parameters of radiation emitted by many particles

We consider a set of field lines on the 2D plane, and estimate the total emission by particles accelerated along them. During pulsar rotation, the sight line stays at a particular θ with respect to the 2D plane. Since the emission from each particle is relativistically beamed in the direction of velocity $\boldsymbol{\beta}$, the observer tends to receive the radiation from all those particles, for which $\boldsymbol{\beta}$ falls with in the angular width of $\pm 1/\gamma$ with respect to $\hat{n}$.

First we estimate the polarization parameters of the radiation emitted by a single particle at the instant $t_0 \le t_{\rm max}$. The instant t_0 is the time at which $\hat{n}\cdot\boldsymbol{\beta} = 1$ for a given initial $\phi_{\rm p}$. As the rotation progresses, new t_0 is computed for the advanced rotation phase by again solving $\hat{n}\cdot\boldsymbol{\beta} = 1$ and computing the polarization parameters. This procedure is continued till $t_0 \approx t_{\rm max}$, where $t_{\rm max}$ is the time at which the particle goes out of radio emission zone ($d_0 \le r \le 3 \times 10^3$ Km). Since the radiation is emitted over a range of r, and due to the aberration and retardation, the radiation beam gets shifted to the leading side of the pulse. The role of retardation and aberration phase shifts has been discussed by e.g., Phillips (1992) and Gangadhara & Gupta (2001).

In order to compute the total polarization parameters with respect to the rotation phase, we first the polarization parameters due to single particles into groups of phase bins and add them. In the following steps, we give the details of the procedure followed:

1. fix the observer's sight line at a specific θ with respect to the 2D plane;
2. select a set of field lines in the range of $-5^\circ \le \phi_{\rm p} \le 5^\circ$ with a successive line spacing of 0.1°;
3. solve $\hat{n}\cdot\hat{\beta} = 1$ to find t_0 at the point of emission on the trajectory corresponding to each field line, and estimate the polarization parameters at those points;
4. subtract the retardation phase shift $\Omega(t_{\rm max} - t_0)$ from η assigned for each of the emission beam, and estimate the effective rotation phase;
5. rotate the sight line by 0.1° to a new phase, and repeat the procedure (1–4) over the range of $-12^\circ \le \eta \le 12^\circ$;
6. finally, sort the array of polarization parameters into groups of phase bins, and add to get the total pulse profile.

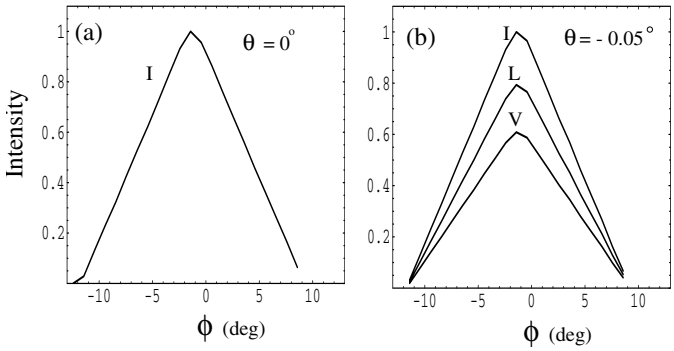

Fig. 6. The simulated profiles: panel **a)** for $\theta = 0°$ and panel **b)** for $\theta = -0.05°$. The parameter ϕ is the rotation phase. Used $\gamma_0 = 100$ and $d_0 = 10$ Km.

In Fig. 6, we give the total polarization parameters computed from the emissions by many particles as functions of rotation phase. In Panel (a) we have plotted the profile that is obtained when the sight line lies in the 2D plane, and Panel (b) for the case when the sight line is inclined by $-0.05°$. The profiles indicate that the peak emissions are shifted to the earlier phase as a consequence of the aberration-retardation effect.

6. Discussion

For simplicity we considered the dipole field lines projected onto a 2D plane. The relativistic particles are assumed to be streaming outward along such a field configuration with an initial Lorentz factor in the range of $10^2 \leq \gamma_0 \leq 10^3$. Since our aim is to understand the rotation effects on particle dynamics and pulse profile, we consider the single particle emission and leave the collective plasma emissions to later works. We are interested in the region which extends from a few stellar radii to a radial distance well within the light cylinder, where the radio emission is expected to occur and the bead-on-wire approximation holds. Though we have approximated the particle motion to 2D, we are able to investigate the influence of rotation on pulsar profiles. Our model is more relevant for those cases where the inclination angle α of the magnetic axis relative to rotation axis is large enough. In such cases, the projected field lines may be approximated to be straight lines over a significant radial distance. We derived an expression for the radial position of a particle (Eq. (20)), which shows an oscillatory behavior, as shown in Fig. 2. A similar case of particle motion in an infinitely long, straight, and rigidly rotating tube, was discussed by considering a gedanken experiment by MR94, who show that due to the centrifugal force reversal, the particle returns back to the rotation axis after reaching a maximum distance at which the rotation velocity reaches the speed of light. This turns out to be an oscillatory motion in the radial direction. Gangadhara (1996) showed that the particle angular velocity cannot be same as the field line angular velocity if the magnetic axis is inclined with respect to the rotation axis. We considered this effect in our treatment of particle motion, and found the particle trajectories and their curvature radii vary with field line orientation.

Since the magnetic field is very strong, the Larmour radius of gyration and drift velocity of the charged particles become very small. So, the particles are assumed to follow the same set of field lines all along their trajectories. In the case of single particle dynamics, the magnetic field dominates so that the rigid body motion may be extended all the way up to the light cylinder. But in reality plasma corotates with the neutron star, and we must take the plasma inertia into account in the region close to the light cylinder. Therefore, it is possible that the magnetic field lines will sweep back and can lead to the generation of toroidal magnetic field. Hence the oscillatory motion that our solution predicts cannot be achieved in a real physical situation like pulsars, and the particle which reaches the vicinity of the light cylinder cannot come back, but escapes from the magnetosphere as a pulsar wind.

We find the energy of particle increases due to the centrifugal force, as indicated by the Eq. (7) for Lorentz factor γ. In this way the rotational energy of neutron star gets transferred to the particles via the magnetic field lines.

We find that the radius of curvature of particle trajectory is approximately $r_L/2$, which is comparable to the inherent radius of curvature of dipolar field lines (Gangadhara 2004). We, therefore believe that curvature emission due to the rotational motion of particles should be comparable to the actual curvature emission in a corotating frame. Both the Lorentz factor and the characteristic frequency reach the maxima in the region close to light cylinder. Our model thus indicates that high frequency radiation (e.g., X-ray, γ-ray) may be emitted in the regions close to light cylinder.

In a later work, Rogava et al. (2003) show that if a particle moves freely along a tube with an arbitrary curvature, the centrifugal force does not always reverse. They show that the particles move in the tube with a variable angular velocity. This supports our result that the particles' angular velocity on some field lines differs from that of pulsar's; that is, the particles moving along the field lines with $\phi_{\rm p} = 0$ rotate with the angular velocity that is same as the pulsar angular velocity. But those moving along other field lines, for which $\phi_{\rm p} \neq 0$, rotate with the angular velocity which is smaller than the pulsar angular velocity. The particles moving along the field lines with $\phi_{\rm p} \sim 0$ tend to emit more power than those moving along other field lines, such that the profile in Fig. 5 shows a peak at $\phi_{\rm p} \sim 0$. Also, it is evident from observations that the peak of pulsar profiles (core) is, probably, emitted from the field lines with $\phi_{\rm p} \sim 0$.

We have reproduced a simulated pulse profile (Fig. 6) adding the radiation emitted by particles accelerated on a set of field lines, by taking aberration-retardation into account. The sign of ϕ has been flipped to match with the phase sign convention followed in pulsar profiles. The roughness in the curves of Fig. 6 are due to the increments of $0.1°$ in $\phi_{\rm p}$ and η. This choice was made based on the limitation in computing time. However, the smoother profiles can always be generated by choosing smaller increments and opting for longer computing time. Since we consider uniform plasma flow along the field lines, our profiles do not have subpulse components.

Our model shows effects, such as aberration and retardation, which make the pulse profiles to become asymmetric about the pulse center. This phenomenon has been observed

in most of the pulsar profiles (e.g., Gangadhara & Gupta 2001; Gupta & Gangadhara 2003).

In our model, we find that if the sight line is at a fixed angle ($\theta = -0.05^\circ$, see Fig. 6) to the particle trajectory plane, the observer tends to receive a single sign circular polarization, as observed in many pulsars (e.g., Han et al. 1998). As a followup to this work, we plan to consider the full 3D dynamics of plasma in a rotating dipolar magnetic field, and estimate the coherent radiation.

7. Conclusion

By considering projected dipolar magnetic field lines on a plane perpendicular to the rotation axis, we have developed a 2D model for the particle dynamics in a pulsar magnetosphere. The motive behind developing this model was to elucidate some of the rotational effects induced in the pulsar profiles. We obtained the analytical expressions for the particle trajectory and its curvature radius. The energy of particles increase at the expense of the neutron star's rotational energy. We find the sight line orientation relative to the particle trajectory plane might determine the sign of circular polarization. The asymmetries observed in the pulse profiles can be explained by considering the aberration-retardation effects.

Acknowledgements. We thank Jayanth Murthy for comments.

References

Abramowitz, M., & Stegun, I. A. 1972, A Hand Book of Mathematical Functions (New York: Dover Publications, Inc.)
Asséo, E., & Riazuelo, A. 2000, MNRAS, 318, 983
Blaskiewicz, M., Cordes, J. M., & Wasserman, I. 1991, ApJ, 370, 643
Buschauer, R., & Benford, G. 1976, MNRAS, 177, 109
Buschauer, R., & Benford, G. 1977, MNRAS, 178, 189
Gangadhara, R. T. 1996, A&A, 314, 853, (G96)
Gangadhara, R. T. 1997, A&A, 327, 155
Gangadhara, R. T., & Gupta, Y. 2001, ApJ, 555, 31
Gangadhara, R. T. 2004, ApJ, 609, 335
Gangadhara, R. T., & Lesch, H. 1997, A&A Lett., 323, 45
Gil, J. A., & Snakowski, J. K. 1990, A&A, 234, 237
Gil, J. A., Lyubarsky, Y., & Melikidze, G. I. 2004, ApJ, 600, 872
Gold, T. 1969, Nature, 221, 25
Gupta, Y., & Gangadhara, R. T. 2003, ApJ, 584, 418
Jackson, J. D. 1972, Classical Electrodynamics (New York: Wiley)
Han, J. L., Manchester, R. N., Xu, R. X., & Qiao, G. J. 1998, MNRAS, 300, 373
Hibschman, J. A., & Arons, J. 2001, ApJ, 546, 382
Karpman, V. I., Norman, C. A., ter Haar, D., & Tsitovich, V. N. 1975, Phys. Scr., 11, 271
Lyne, A. G., & Manchester, R. N. 1988, MNRAS, 234, 477
Machabeli, G. Z., & Rogava, A. D. 1994, Phys. Rev. A, 50, 98, (MR94)
Melrose, D. B., & Gedalin, M. E. 1999, ApJ, 521, 351
Pearson, C. E. 1974, Hand Book of Applied Mathematics (Van Nostrand Rienhold Company), 372
Peyman, A., & Gangadhara, R. T. 2002, ApJ, 566, 365
Phillips, J. A. 1992, ApJ, 385, 282
Rieger, F. M., & Mannheim, K. 2000, A&A, 353, 473
Rogava, A. D., Dalakishvili, G., & Osmanov, Z. 2003, Gen. Rel. Grav., 35, 1133 [arXiv:astro-ph/0303604]
Ruderman, M., & Sutherland, P. 1975, ApJ, 196, 51, (RS75)
Stinebring, D. R., Cordes, J. M., Rankin, J. M., Wiesberg, J. M., & Boriakoff, V. 1984, ApJS, 55, 247
Sturrock, P. A. 1971, ApJ, 164, 529
Thomas, R. M. C., & Gangadhara, R. T. 2005 [arXiv:astro-ph/0501315]
Zwillinger, D. 1989, Hand Book of Differential Equations, (N.Y. Academic Press Inc.), 153

Online Material

Appendix A: To find a series expansion for the factor $\hat{n}\times(\hat{n}\times\boldsymbol{\beta})$ that appears in Eq. (32)

Consider $\boldsymbol{\beta}$ in Cartesian co-ordinates:

$$\boldsymbol{\beta} = \frac{1}{c}(V_x\hat{x} + V_y\hat{y}), \tag{A.1}$$

where $\hat{x}$ and $\hat{y}$ are the unit vectors along the x and y-axes, respectively, (Fig. 1). Then it follows from Eq. (2) that

$$V_x = V_r\cos\left(\frac{\phi_{\rm tot}(t+t_0)}{2}\right) - V_\phi\sin\left(\frac{\phi_{\rm tot}(t+t_0)}{2}\right), \tag{A.2}$$

and

$$V_y = V_r\sin\left(\frac{\phi_{\rm tot}(t+t_0)}{2}\right) + V_\phi\cos\left(\frac{\phi_{\rm tot}(t+t_0)}{2}\right). \tag{A.3}$$

Using Eq. (37), we derive the series expansions for radial velocity V_r and rotation velocity V_ϕ:

$$V_r = \frac{{\rm d}r}{{\rm d}t}, \tag{A.4}$$

$$V_\phi = r\Omega^*. \tag{A.5}$$

By substituting V_r and V_ϕ into by Eqs. (A.2) and (A.3), we obtain

$$\begin{aligned} V_x &= V_{x0} + V_{x1}t + V_{x2}t^2, \\ V_y &= V_{y0} + V_{y1}t + V_{y2}t^2 .... \end{aligned} \tag{A.6}$$

The expressions of V_{x0}, V_{y0}, V_{x1}, V_{y1} ... in the above expansions are lengthy (see Thomas & Gangadhara 2005). Using the triple vector identity and the definitions of $\hat{n}$, $\hat{\epsilon}_\parallel$ and $\hat{\epsilon}_\perp$, we obtain

$$\hat{n}\times(\hat{n}\times\boldsymbol{\beta}) = -(\boldsymbol{\beta}.\,\hat{\epsilon}_\parallel)\,\hat{\epsilon}_\parallel - (\boldsymbol{\beta}.\,\hat{\epsilon}_\perp)\,\hat{\epsilon}_\perp, \tag{A.7}$$

where

$$\boldsymbol{\beta}\cdot\hat{\epsilon}_\parallel = -\frac{\sin\theta}{c}\left(V_y\sin\eta + V_x\cos\eta\right), \tag{A.8}$$

$$\boldsymbol{\beta}\cdot\hat{\epsilon}_\perp = \frac{1}{c}(V_y\cos\eta - V_x\sin\eta). \tag{A.9}$$

Using the series expansions of V_x and V_y, we write

$$\begin{aligned} \hat{n}\times(\hat{n}\times\boldsymbol{\beta}) = \frac{1}{c}\Big[&\hat{\epsilon}_\parallel\sin\theta\left(V_{\parallel 0} + V_{\parallel 1}t + V_{\parallel 2}t^2\right) \\ &+\hat{\epsilon}_\perp(V_{\perp 0} + V_{\perp 1}t + V_{\perp 2})\Big], \end{aligned} \tag{A.10}$$

where

$$V_{\parallel i} = V_{yi}\sin\eta + V_{xi}\cos\eta, \tag{A.11}$$

$$V_{\perp i} = V_{xi}\sin\eta - V_{yi}\cos\eta, \tag{A.12}$$

and $i = 0, 1, 2$.

Appendix B: Transformations for solving Eq. (32)

Using the method of Buschauer & Benford (1976), we make the following transformations in order to solve the integral in Eq. (32).

Consider

$$\begin{aligned} \int_{-\infty}^{\infty}\exp\left[{\rm i}\left(N_1t + N_2t^2 + N_3t^3\right)\right]{\rm d}t = \\ \frac{1}{N_3^{1/3}}{\rm e}^{iC_{\rm n}}\int_{-\infty}^{\infty}\exp[{\rm i}\left(z\tau + \tau^3\right)]\,{\rm d}\tau, \end{aligned} \tag{B.1}$$

where

$$\tau = \frac{1}{N_3^{1/3}}\left(t + \frac{N_2}{3N_3}\right) \tag{B.2}$$

is a dimensionless variable, and

$$z = \frac{1}{N_3^{1/3}}\left(N_1 - \frac{N_2^2}{3N_3}\right). \tag{B.3}$$

By differentiating the Eq. (B.1) with respect to N_1 and N_2, we obtain

$$\begin{aligned} \int_{-\infty}^{\infty} t\,\exp[{\rm i}(N_1t + N_2t^2 + N_3t^3)]\,{\rm d}t = \\ \frac{1}{N_3^{2/3}}{\rm e}^{{\rm i}C_{\rm n}}\Big[\int_{-\infty}^{\infty}\tau\,\exp\left[{\rm i}\left(z\tau + \tau^3\right)\right]{\rm d}\tau - C_l\int_{-\infty}^{\infty}\exp\left[{\rm i}\left(z\tau + \tau^3\right)\right]{\rm d}\tau\Big] \end{aligned} \tag{B.4}$$

and

$$\begin{aligned} \int_{-\infty}^{\infty} t^2\exp\left[{\rm i}\left(N_1t + N_2t^2 + N_3t^3\right)\right]{\rm d}t = \\ \frac{1}{N_3^{1/3}}{\rm e}^{{\rm i}C_{\rm n}}\Big[C_{\rm m}\int_{-\infty}^{\infty}\exp\left[{\rm i}\left(z\tau + \tau^3\right)\right]{\rm d}\tau \\ +C_{\rm p}\int_{-\infty}^{\infty}\tau\exp\left[{\rm i}\left(z\tau + \tau^3\right)\right]{\rm d}\tau\Big]. \end{aligned} \tag{B.5}$$

We define

$$\begin{aligned} L_1(z) &= \int_{-\infty}^{\infty}\exp\left[{\rm i}\left(z\tau + \tau^3\right)\right]{\rm d}\tau \\ &= \frac{2}{3}\sqrt{z}\,{\rm K}_{1/3}\left[2(z/3)^{3/2}\right], \end{aligned} \tag{B.6}$$

$$\begin{aligned} L_2(z) &= \int_{-\infty}^{\infty}\tau\exp\left[{\rm i}\left(z\tau + \tau^3\right)\right]{\rm d}\tau \\ &= {\rm i}\frac{2}{\sqrt{27}}\,z\,{\rm K}_{2/3}\left[2(z/3)^{3/2}\right], \end{aligned} \tag{B.7}$$

$$B_0 = \frac{1}{N_3^{1/3}}{\rm e}^{{\rm i}C_{\rm n}}{\rm L}_1(z), \tag{B.8}$$

$$B_1 = \frac{1}{N_3^{2/3}} \mathrm{e}^{\mathrm{i}C_\mathrm{n}} [\mathrm{L}_2(z) - C_\mathrm{l}\mathrm{L}_1(z)], \tag{B.9}$$

$$B_2 = \frac{1}{N_3^{1/3}} \mathrm{e}^{\mathrm{i}C_\mathrm{n}} \left[C_\mathrm{m}\mathrm{L}_1(z) - C_\mathrm{p}\mathrm{L}_2(z)\right], \tag{B.10}$$

where

$$C_l = \frac{N_2}{3N_3^{2/3}}, \tag{B.11}$$

$$C_n = \frac{N_2}{3N_3}\left[\frac{2N_2^2}{9N_3} - N_1\right], \tag{B.12}$$

$$C_m = \left[\frac{2N_2^2}{9N_3^2} - \frac{N_1}{3N_3}\right], \tag{B.13}$$

$$C_p = \frac{2N_2}{3N_3^{4/3}}. \tag{B.14}$$